

## Article

# Interfacial Effect on Photo-Modulated Magnetic Properties of Core/Shell-Structured NiFe/NiFe<sub>2</sub>O<sub>4</sub> Nanoparticles

Wenda Zhou <sup>1,2</sup>, Mingyue Chen <sup>1,2</sup>, He Huang <sup>1</sup>, Guyue Wang <sup>1</sup>, Xingfang Luo <sup>2</sup>, Cailei Yuan <sup>2,\*</sup> , Jingyan Zhang <sup>1</sup>, Yanfei Wu <sup>1</sup>, Xinqi Zheng <sup>1</sup>, Jianxin Shen <sup>1</sup>, Shouguo Wang <sup>1,\*</sup> and Baogen Shen <sup>1,3,4,\*</sup>

<sup>1</sup> School of Materials Science and Engineering, Beijing Advanced Innovation Center for Materials Genome Engineering, University of Science and Technology Beijing, Beijing 100083, China;

wdzhou@xs.ustb.edu.cn (W.Z.); mychen@xs.ustb.edu.cn (M.C.); hhuang@ustb.edu.cn (H.H.);

ywang@xs.ustb.edu.cn (G.W.); jy Zhang@ustb.edu.cn (J.Z.); yanfeiwu@ustb.edu.cn (Y.W.);

zhengxq@ustb.edu.cn (X.Z.); jxshen@ustb.edu.cn (J.S.)

<sup>2</sup> Jiangxi Key Laboratory of Nanomaterials and Sensors, School of Physics, Communication and Electronics, Jiangxi Normal University, Nanchang 330022, China; xfluo@jxnu.edu.cn

<sup>3</sup> Beijing National Laboratory for Condensed Matter Physics, Institute of Physics, Chinese Academy of Sciences & University of Chinese Academy of Sciences, Beijing 100190, China

<sup>4</sup> Institute of Rare Earths, Chinese Academy of Sciences, Ganzhou 341000, China

\* Correspondence: clyuan@jxnu.edu.cn (C.Y.); sgwang@ustb.edu.cn (S.W.); shenbg@iphy.ac.cn (B.S.)

**Abstract:** Photo-modulated magnetism has become an emerging method for technological applications, such as magneto-optical devices. In this work, by introducing oxygen during rapid thermal annealing, NiFe/NiFe<sub>2</sub>O<sub>4</sub> core/shell nanoparticles were successfully fabricated by pulsed laser deposition. Obvious photo-modulated ferromagnetism was observed in core/shell nanoparticles confined in Al<sub>2</sub>O<sub>3</sub> film. Theoretical and experimental investigations indicate much more photogenerated electrons are captured at the interface of NiFe/NiFe<sub>2</sub>O<sub>4</sub> compared with NiFe nanoparticles due to interfacial effect, resulting in the improved ferromagnetism under light irradiation. This work provides a promising strategy for optical engineering design of optical information storage, high-speed wireless communication, and magneto-optical semiconductor devices.

**Keywords:** bimagnetic core/shell; interfacial effect; photo-modulation



**Citation:** Zhou, W.; Chen, M.; Huang, H.; Wang, G.; Luo, X.; Yuan, C.; Zhang, J.; Wu, Y.; Zheng, X.; Shen, J.; et al. Interfacial Effect on Photo-Modulated Magnetic Properties of Core/Shell-Structured NiFe/NiFe<sub>2</sub>O<sub>4</sub> Nanoparticles. *Materials* **2022**, *15*, 1347. <https://doi.org/10.3390/ma15041347>

Academic Editor: Agnieszka Jastrzębska

Received: 31 December 2021

Accepted: 9 February 2022

Published: 11 February 2022

**Publisher's Note:** MDPI stays neutral with regard to jurisdictional claims in published maps and institutional affiliations.



**Copyright:** © 2022 by the authors. Licensee MDPI, Basel, Switzerland. This article is an open access article distributed under the terms and conditions of the Creative Commons Attribution (CC BY) license (<https://creativecommons.org/licenses/by/4.0/>).

## 1. Introduction

Bimagnetic core/shell nanocomposites have attracted particular attention because of their promising application prospects in diverse fields, such as magnetic devices, biomedicine, energy storage, and spin-related catalysis [1–8]. In fact, core/shell architecture has been considered an attractive approach to developing novel properties of various nanomaterials [9–11]. For the material design of bimagnetic nanocrystals, in addition to integrating the characteristics of the core and shell, interfacial exchange (interfacial effect) is vital for the eventual realization of designed and tunable functionalities [12–14]. However, a fundamental understanding of the core/shell interfacial effect remains a major challenge. On the other hand, tunable magnetism is one of the most widely studied issues in the application and development of spintronics [15–18]. It has been proposed that many strategies such as magnetic field, spin-orbit engineering, thermal gradient, chemical functionalization, strain, and electric field are greatly helpful to realize the manipulation of magnetism [15–20]. Apart from the aforementioned modulation techniques, photo-modulation of magnetism has become an emerging method for technological applications, especially in high-speed wireless communication [21–25]. This approach has the advantages of large storage capacity and low cost, which has attracted extensive research recently [22–26]. In this case, although the interfacial electronic structure of core/shell architecture inherently affects the magnetic properties of bimagnetic nanoparticles and provides an ideal platform for

optical adjustment function, the photo-modulation of magnetism in bimagnetic core/shell nanoparticles remains a relatively unexplored area.

Permalloy (NiFe) is a typical soft magnetic material widely used in transformer cores and magnetic recording heads [27]. Nickel ferrite ( $\text{NiFe}_2\text{O}_4$ ) with a high Curie temperature and tunable bandgap are applicable in magnetic refrigeration, magnetic resonance imaging, biomedical applications, and catalysis [25,28,29]. Integrating both materials to create bimagnetic core/shell nanocomposites may bring innovative properties and intriguing applications [30]. More interestingly, this bimagnetic core/shell nanocomposite may also provide a platform for photo-modulation by interfacial effect. In this work, the NiFe/ $\text{NiFe}_2\text{O}_4$  core/shell nanoparticles were prepared through a pulsed laser deposition (PLD) technique and rapid thermal annealing under an oxygen atmosphere. With the interfacial effect of core-shell structure, the magnetic properties of NiFe/ $\text{NiFe}_2\text{O}_4$  nanoparticles can be significantly manipulated by photo-illumination, but no obvious change in NiFe nanoparticles under photo-illumination. Density functional theory (DFT) calculation indicates that the photo-modulated effect is associated with the charge accumulations at the interface of core/shell architecture. The robust photo-modulated ferromagnetism can help accomplish high-speed and wireless nonvolatile storage and logic operations. This work demonstrates the tunability of the core/shell interfacial effect and expands the potential applications of bimagnetic nanoparticles to optical information storage and semiconductor spintronics.

## 2. Materials and Methods

NiFe/ $\text{NiFe}_2\text{O}_4$  nanoparticles confined in  $\text{Al}_2\text{O}_3$  films were synthesized by the PLD system (LMBE450A, SKY, Shenyang, China) and rapid thermal annealing. Briefly, the NiFe target (10 mm  $\times$  20 mm, 99.99% purity) was glued to the  $\text{Al}_2\text{O}_3$  target (60 mm in diameter, 99.99% purity) by silver glue. The p-type Si substrates were cleaned with deionized water and followed by acetone. During the deposition process, the assembled NiFe/ $\text{Al}_2\text{O}_3$  target rotated slowly around the central axis, and these two components were evaporated to Si substrate alternately by a laser beam. The composite target was ablated by KrF pulsed laser with a wavelength of 248 nm for 15 min after the chamber pumped down to  $1.5 \times 10^{-7}$  Torr. During the deposition, the composite target was slowly rotated. Then, the samples were annealed at 600 °C for 120 s under oxygen partial pressure of about 1 Pa. The synthesis condition of NiFe nanoparticles is the same as NiFe/ $\text{NiFe}_2\text{O}_4$  nanoparticles, but without oxygen during the rapid thermal annealing process. Transmission electron microscopy (TEM) characterizations were performed by FEI Talos f200 $\times$  (Thermo Fisher, Waltham, MA, USA) microscope operated at 200 kV. X-ray photoelectron spectroscopy (XPS) was examined using the XSAM800 spectrometer (Kratos, Manchester, UK) employing Al K $\alpha$  radiation. The XPS binding energies were calibrated by the C 1s peak (284.8 eV). The physical property measurement system (PPMS, Ever Cool II, Quantum Design, San Diego, CA, USA) with a vibrating sample magnetometer option was used to investigate the magnetic properties of the synthesized samples.

## 3. Results and Discussion

Figure 1a shows the low magnification TEM image of as-synthesized NiFe/ $\text{Al}_2\text{O}_3$  nanofilm. Obviously, several NiFe nanoparticles with an average size of ~20 nm can be observed in the amorphous  $\text{Al}_2\text{O}_3$  matrix. As shown in Figure 1b, the selected area electron diffraction (SAED) pattern of NiFe nanoparticles shows a good match with the simulated results obtained by TEM simulator software (JAVA Electron Microscope Simulation (JEMS)) [24]. It clearly demonstrates that the NiFe nanoparticle has a cubic structure with the  $p4/mmm$  space group (Figure 1d). The high-resolution TEM (HRTEM) image in Figure 1c further shows the successful formation of NiFe nanoparticles with a size of about 20 nm, and the inter-planar spacing (0.205 nm) corresponds to the (111) crystal plane of NiFe [31]. By introducing oxygen during rapid thermal annealing, the NiFe/ $\text{NiFe}_2\text{O}_4$  core/shell nanoparticles can be successfully fabricated, as shown in Figure 1e. The average

size of NiFe/NiFe<sub>2</sub>O<sub>4</sub> core/shell nanoparticles is ~20 nm found from Figure S1 (the histogram of the NiFe/NiFe<sub>2</sub>O<sub>4</sub> nanoparticles size distribution in Supporting Information). As shown in Figure 1f, the diffraction patterns for NiFe and NiFe<sub>2</sub>O<sub>4</sub> match with their simulated diffraction patterns by TEM JEMS software. The experimental and simulated electron diffraction patterns confirmed that the core/shell nanoparticles consisted of cubic NiFe (space group *p4/mmm*) and cubic NiFe<sub>2</sub>O<sub>4</sub> (space group *Fd-3mS*, Figure 1h). The HRTEM image (Figure 1g) reveals that the NiFe/NiFe<sub>2</sub>O<sub>4</sub> core/shell structure is composed of a single crystal NiFe core and uniform polycrystalline NiFe<sub>2</sub>O<sub>4</sub> shell with different lattice orientations [32]. It is reasonable to conclude that the oxidation only takes place on the surface of NiFe nanoparticles, rather than penetrating the internal NiFe nanoparticles during the annealing process to form NiFe<sub>2</sub>O<sub>4</sub> shell. Besides, the formation of NiFe<sub>2</sub>O<sub>4</sub> shell is also confirmed by Raman spectra (Figure S2 in Supporting Information) [25]. Therefore, by adjusting the oxygen atmosphere, the microstructures and morphologies of nanoparticles can be significantly influenced, and the growth of NiFe and NiFe/NiFe<sub>2</sub>O<sub>4</sub> core/shell structure can be well controlled.

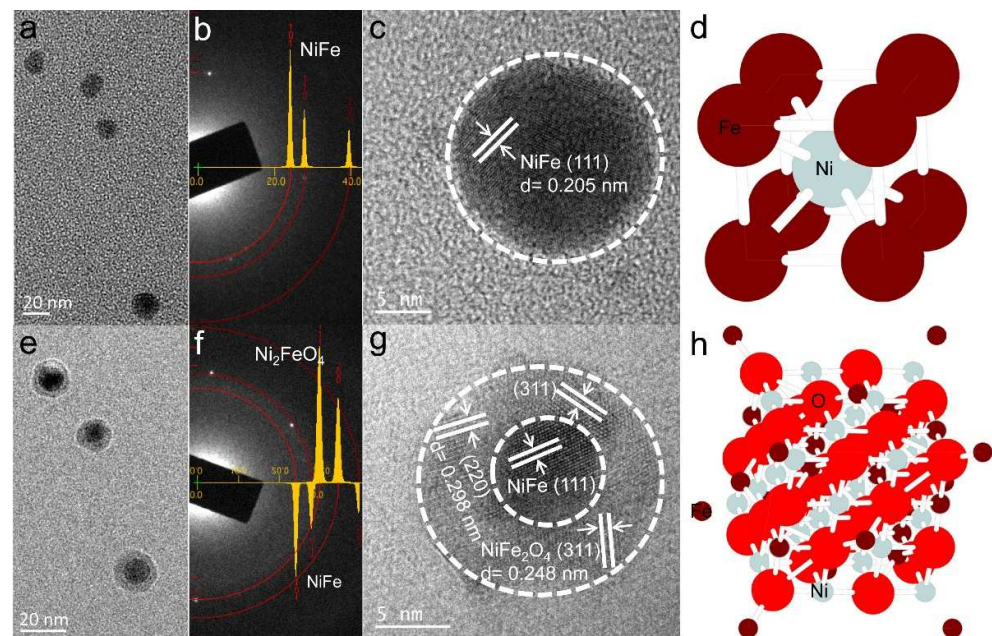


**Figure 1.** (a,e) lanar low magnitude TEM images, (b,f) electron diffraction patterns, (c,g) HRTEM images, (d,h) unit cell schematic diagrams of NiFe nanoparticles and NiFe/NiFe<sub>2</sub>O<sub>4</sub> core/shell nanoparticles in amorphous Al<sub>2</sub>O<sub>3</sub> matrix, respectively.

XPS technique was adopted to clarify the chemical compositions and stoichiometry of NiFe and NiFe<sub>2</sub>O<sub>4</sub> nanoparticles in the Al<sub>2</sub>O<sub>3</sub> matrix. As displaced in Figure 2a, for NiFe in the Al<sub>2</sub>O<sub>3</sub> matrix, the binding energy of Ni 2p<sub>3/2</sub> and Ni 2p<sub>1/2</sub> core level is located at 852.6 eV and 870.1 eV, respectively, where its satellite peaks at 859.0 eV and 876.9 eV indicate a Ni<sup>0</sup> valence state in NiFe [33]. Likewise, the binding energy of Fe 2p<sub>3/2</sub> and Fe 2p<sub>1/2</sub> locates at about 706.6 and 720.5 eV (Figure 2b), respectively, in good agreement with the Fe<sup>0</sup> counterpart reported before [34]. Besides, the main peak of O 1s is centered at 529.0 eV (Figure 2c) and of Al 2p at 72.4 eV (Figure 2d) for NiFe in Al<sub>2</sub>O<sub>3</sub> matrix implies that NiFe shows no chemical interaction with the surrounding Al<sub>2</sub>O<sub>3</sub> matrix [24], in agreement with the TEM results. In the case of NiFe<sub>2</sub>O<sub>4</sub> nanoparticles in the Al<sub>2</sub>O<sub>3</sub> matrix, the XPS spectra of Ni 2p and Fe 2p were also included. As shown in Figure 2e, the main band of Ni 2p<sub>3/2</sub> (853.8 eV) was well fitted with two peaks centered at 853.7eV and 854.6eV. Ni 2p<sub>1/2</sub> was situated at 871.6 eV, accompanied by satellite peaks on the left side of the main peaks, which matched well with the corresponding values for the Ni<sup>2+</sup> state previously reported [25]. The Fe 2p<sub>3/2</sub> and Fe 2p<sub>1/2</sub> spectra shown in Figure 2e present a pair of key

peaks centered at 710.9 and 724.7 eV, except that a significant satellite peak related with typical  $\text{Fe}^{3+}$  at 718.5 eV [25,34]. It is more worthwhile to note that Ni 2p and Fe 2p spectra in  $\text{NiFe}_2\text{O}_4$  nanocrystals show a positive shift of binding energy compared to NiFe, denoting higher valence states of Ni and Fe in  $\text{NiFe}_2\text{O}_4$  nanocrystals [34]. Meanwhile, it also shows no chemical interaction with the surrounding  $\text{Al}_2\text{O}_3$  matrix since the binding energy of the Al 2p spectrum is centered at 72.7 eV, and that of the O 1s spectrum is centered at 529.4 eV. Thus, the formation of NiFe/ $\text{NiFe}_2\text{O}_4$  core/shell nanoparticles confined in the  $\text{Al}_2\text{O}_3$  matrix was further demonstrated by XPS results.

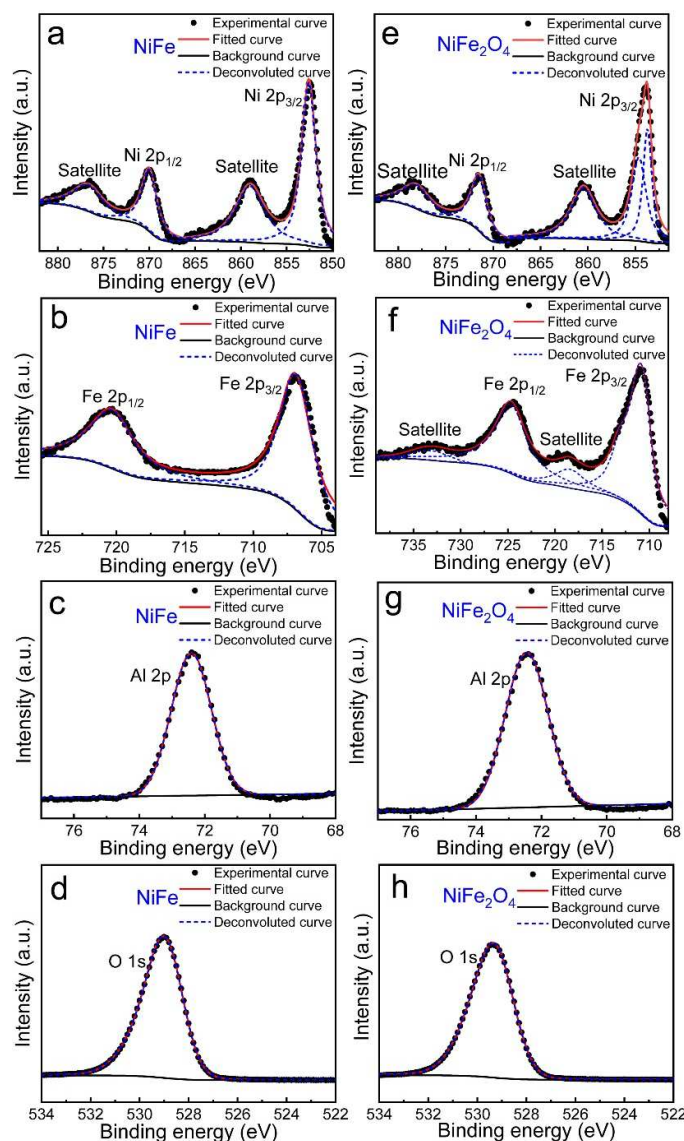


**Figure 2.** XPS spectra of (a,e) Ni 2p, (b,f) Fe 2p, (c,g) Al 2p, (d,h) O 1s of NiFe nanoparticles and NiFe/ $\text{NiFe}_2\text{O}_4$  core/shell nanoparticles, respectively.

To characterize the ferromagnetic properties of NiFe nanoparticles and NiFe/ $\text{NiFe}_2\text{O}_4$  core/shell nanoparticles, the measurement of field cooling (FC) and zero-field cooling (ZFC) modes from 5 K to 300 K were carried out, respectively. As shown in the ZFC curves in Figure 3a,d, both nanoparticles display a peak near the blocking temperature ( $T_B$ ). The ZFC curves are obviously separated from the FC curve below  $T_B$ . Figure 3b,e show the magnetic-field dependent magnetization (M-H) measurements of NiFe nanoparticles and NiFe/ $\text{NiFe}_2\text{O}_4$  core/shell nanoparticles at 10 K and 300 K, respectively. No significant hysteresis was observed for both samples at 300 K. However, at 10 K, obvious hysteresis

can be seen for both samples with magnetic hysteresis loops, indicating the ferromagnetic behaviors. The M-T and M-H curves under light irradiation (530 nm,  $\sim 0.75$  mW/cm<sup>2</sup>) were also shown in Figure 3d. Interestingly, under light irradiation, the M-T curve of NiFe/NiFe<sub>2</sub>O<sub>4</sub> core/shell nanoparticles shows a much more obvious change compared with that of NiFe, where  $T_B$  is increased from  $\sim 16$  K to  $\sim 22$  K. Furthermore, it is worth noting that the saturation magnetization of NiFe/NiFe<sub>2</sub>O<sub>4</sub> core/shell nanoparticles becomes larger under light irradiation. Meanwhile, M-T and M-H curves of NiFe nanoparticles show negligible change under light irradiation. Moreover, after turning off the light, the magnetization of both samples recovers rapidly to its no-light irradiation case. The above results clearly demonstrate that the magnetic change of NiFe/NiFe<sub>2</sub>O<sub>4</sub> core/shell nanoparticles is purely electronic, unrelated to light or heat-induced structural or chemical changes [24]. Therefore, based on the above results, it can be inferred that the photogenerated electrons at the core/shell structure interface can improve ferromagnetism and  $T_B$ .

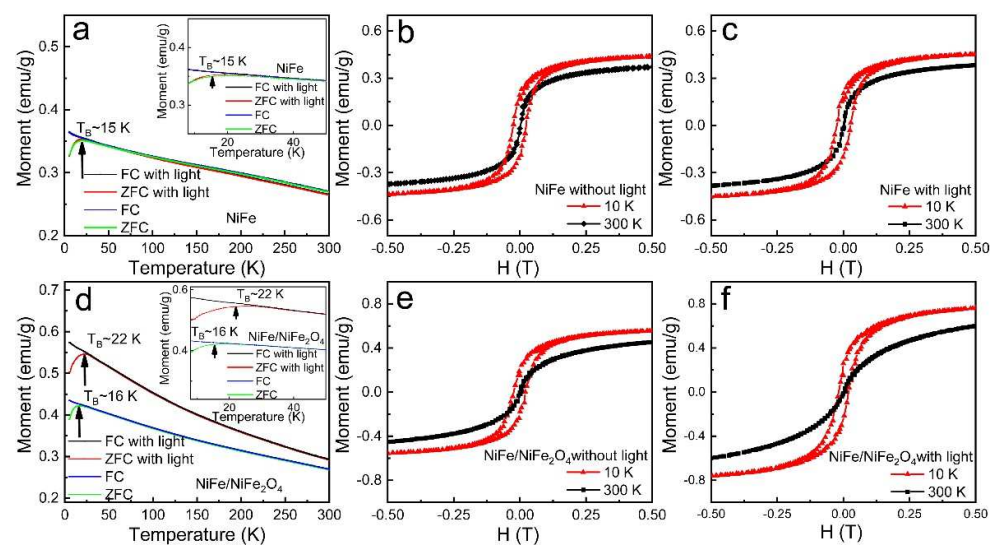


**Figure 3.** M–T curves (a,d), M–H curves (b,c,e,f) for NiFe nanoparticles and NiFe/NiFe<sub>2</sub>O<sub>4</sub> core/shell nanoparticles with and without light, respectively. Inset of (a,d): corresponding magnified images of M–T curve at low-temperature range.

In order to gain further insight into the enhanced ferromagnetism and  $T_B$  of NiFe/NiFe<sub>2</sub>O<sub>4</sub> core/shell nanoparticles under light irradiation, the first-principles calculation was further carried out to investigate the electronic distribution at the interface of NiFe/NiFe<sub>2</sub>O<sub>4</sub>. The DFT calculation in this work was conducted using the Vienna ab initio simulation package (VASP) [35]. The interactions between core and electrons were described by employing the projector augmented wave (PAW) model with the Perdew–Burke–Ernzerhof (PBE) functional [36,37]. The plane wave expansion of the electronic wave function was set to an energy cutoff of 450 eV. Gamma-point centered Monkhorst–Pack grids of  $2 \times 3 \times 1$  k-point mesh were used to calculate slab geometry optimization. The number of atoms included in the calculations was 174. Lattice parameters were as follows:  $a = 17.33$  Å,  $b = 12.92$  Å and  $c = 27.72$  Å. A vacuum layer of 15 Å thickness was added in the  $c$  direction. The force convergence criterion of  $0.02$  eV/Å and the energy convergence criterion of  $10^{-5}$  eV were set, respectively. The side and top views of calculated charge transfer and electron redistribution of NiFe/NiFe<sub>2</sub>O<sub>4</sub> heterostructure are shown in Figure 4. It clearly shows that there is an obvious charge accumulation on the NiFe<sub>2</sub>O<sub>4</sub> side at the interface of NiFe/NiFe<sub>2</sub>O<sub>4</sub>. Moreover, the density of states (DOS) of NiFe/NiFe<sub>2</sub>O<sub>4</sub> core/shell nanoparticle (Figure S3 in Supplementary Materials) manifests the orbital hybridization effect on the interface, which may cause electron redistribution. Therefore, under light irradiation, much more photogenerated electrons are captured at the interface of NiFe/NiFe<sub>2</sub>O<sub>4</sub>, which improves

the lower coordination of surface atoms, partially overcomes the surface spin disorder, and enhances ferromagnetism [24].

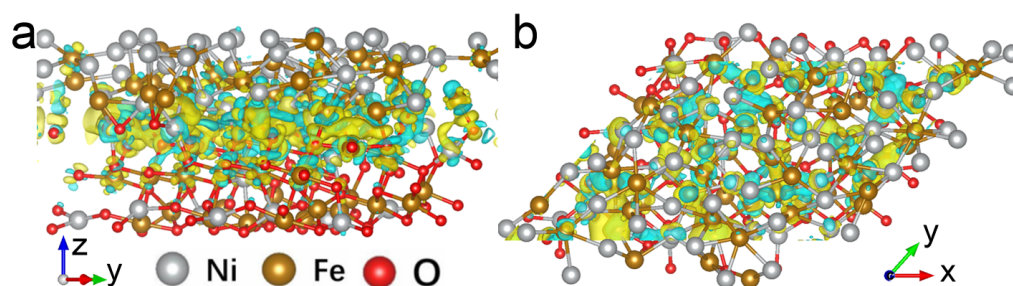


**Figure 4.** (a) Side and (b) top view of calculated charge density difference at the interface of NiFe and NiFe<sub>2</sub>O<sub>4</sub>. The blue and yellow regions represent electron depletion and accumulation, respectively.

#### 4. Conclusions

In summary, NiFe/NiFe<sub>2</sub>O<sub>4</sub> core/shell nanoparticles were successfully synthesized by introducing oxygen during rapid thermal annealing. Obvious photo-modulated ferromagnetism was observed in core/shell nanoparticles confined in Al<sub>2</sub>O<sub>3</sub> film. Given the interfacial effect, much more photogenerated electrons are captured at the interface, and the ferromagnetism of NiFe/NiFe<sub>2</sub>O<sub>4</sub> core/shell nanoparticles can be improved by light irradiation. This work provides a promising strategy for the optical engineering design of optical information storage and magneto-optical coupling devices.

**Supplementary Materials:** The following supporting information can be downloaded at: <https://www.mdpi.com/article/10.3390/ma15041347/s1>, Figure S1: Size distribution; Figure S2: Raman spectra; Figure S3: Calculated DOS of NiFe/NiFe<sub>2</sub>O<sub>4</sub> core/shell nanoparticles.

**Author Contributions:** Conceptualization, C.Y., S.W., and B.S.; software, H.H.; methodology, X.L., J.Z., Y.W., X.Z., and J.S.; investigation, W.Z., M.C., and G.W.; data curation, W.Z.; writing—original draft preparation, W.Z.; writing—review and editing, C.Y. and S.W.; supervision, S.W.; All authors have read and agreed to the published version of the manuscript.

**Funding:** This work was supported by the National Key Research and Development Program of China (Grant No. 2019YFB2005800), the Natural Science Foundation of China (Grants No. 52061017, 52088101, 52130103, and 51971026), the ISF-NSFC Joint Research Program (Grant No. 51961145305), the State Key Laboratory for Advanced Metals and Materials (Grant No. 2019Z-10), Beijing Natural Science Foundation Key Program (Grant No. Z190007), the Fundamental Research Funds for the Central Universities (Grant No. FRF-TP-16-001C2), and Key Program of the Chinese Academy of Sciences (Grants No. 112111KYSB20180013 and QYZDY-SSW-SLH020).

**Institutional Review Board Statement:** Not applicable.

**Informed Consent Statement:** Not applicable.

**Data Availability Statement:** Not applicable.

**Conflicts of Interest:** The authors declare no conflict of interest.

#### References

1. Estrader, M.; López-Ortega, A.; Estradé, S.; Golosovsky, I.V.; Salazar-Alvarez, G.; Vasilakaki, M.; Trohidou, K.N.; Varela, M.; Stanley, D.C.; Sinko, M.; et al. Robust antiferromagnetic coupling in hard-soft bi-magnetic core/shell nanoparticles. *Nat. Commun.* **2013**, *4*, 2960. [[CrossRef](#)] [[PubMed](#)]
2. Zeng, H.; Li, J.; Wang, Z.L.; Liu, J.P.; Sun, S. Bimagnetic core/shell FePt/Fe<sub>3</sub>O<sub>4</sub> nanoparticles. *Nano Lett.* **2004**, *4*, 187–190. [[CrossRef](#)]
3. Lavorato, G.C.; Das, R.; Xing, Y.; Robles, J.; Litterst, F.J.; Baggio-Saitovitch, E.; Phan, M.; Srikanth, H. Origin and shell-driven optimization of the heating power in core/shell bimagnetic nanoparticles. *ACS Appl. Nano Mater.* **2020**, *3*, 1755–1765. [[CrossRef](#)]
4. Omelyanchik, A.; Villa, S.; Vasilakaki, M.; Singh, G.; Ferretti, A.M.; Ponti, A.; Canepa, F.; Margaritis, G.; Trohidou, K.N.; Peddis, D. Interplay between inter- and intraparticle interactions in bi-magnetic core/shell nanoparticles. *Nanoscale Adv.* **2021**, *3*, 6912–6924. [[CrossRef](#)]

5. Song, Q.; Zhang, Z.J. Controlled synthesis and magnetic properties of bimagnetic spinel ferrite  $\text{CoFe}_2\text{O}_4$  and  $\text{MnFe}_2\text{O}_4$  nanocrystals with core-shell architecture. *J. Am. Chem. Soc.* **2012**, *134*, 10182–10190. [[CrossRef](#)]
6. Fabris, F.; Lima, E.; De Biasi, E.; Troiani, H.E.; Mansilla, M.V.; Torres, T.E.; Pacheco, R.F.; Ibarra, M.R.; Goya, G.F.; Zysler, R.D.; et al. Controlling the dominant magnetic relaxation mechanisms for magnetic hyperthermia in bimagnetic core-shell nanoparticles. *Nanoscale* **2019**, *11*, 3164–3172. [[CrossRef](#)]
7. Campos, A.F.C.; de Oliveira, H.A.L.; da Silva, F.N.; da Silva, F.G.; Coppola, P.; Aquino, R.; Mezzi, A.; Depeyrot, J. Core-shell bimagnetic nanoadsorbents for hexavalent chromium removal from aqueous solutions. *J. Hazard. Mater.* **2019**, *362*, 82–91. [[CrossRef](#)]
8. Niether, C.; Faure, S.; Bordet, A.; Deseure, J.; Chatenet, M.; Carrey, J.; Chaudret, B.; Rouet, A. Improved Water Electrolysis Using Magnetic Heating of FeC–Ni Core–Shell Nanoparticles. *Nat. Energy* **2018**, *3*, 476–483. [[CrossRef](#)]
9. Zeng, H.; Sun, S.; Li, J.; Wang, Z.L.; Liu, J.P. Tailoring magnetic properties of core/shell nanoparticles. *Appl. Phys. Lett.* **2004**, *85*, 792–794. [[CrossRef](#)]
10. Wang, F.; Deng, R.; Wang, J.; Wang, Q.; Han, Y.; Zhu, H.; Chen, X.; Liu, X. Tuning upconversion through energy migration in core-shell nanoparticles. *Nat. Mater.* **2011**, *10*, 968–973. [[CrossRef](#)]
11. Ghosh Chaudhuri, R.; Paria, S. Core/shell nanoparticles: Classes, properties, synthesis mechanisms, characterization, and applications. *Chem. Rev.* **2012**, *112*, 2373–2433. [[CrossRef](#)] [[PubMed](#)]
12. Shen, Y.; Lin, Y.H.; Nan, C.W. Interfacial effect on dielectric properties of polymer nanocomposites filled with core/shell-structured particles. *Adv. Funct. Mater.* **2007**, *17*, 2405–2410. [[CrossRef](#)]
13. Wei, P.; Lee, S.; Lemaitre, F.; Pinel, L.; Cutaia, D.; Cha, W.; Katmis, F.; Zhu, Y.; Heiman, D.; Hone, J.; et al. Strong interfacial exchange field in the graphene/EuS heterostructure. *Nat. Mater.* **2016**, *15*, 711–716. [[CrossRef](#)] [[PubMed](#)]
14. Gomez-Perez, J.M.; Zhang, X.P.; Calavalle, F.; Ilyn, M.; González-Orellana, C.; Gobbi, M.; Rogero, C.; Chuvilin, A.; Golovach, V.N.; Hueso, L.E.; et al. Strong interfacial exchange field in a heavy metal/ferromagnetic insulator system determined by spin Hall magnetoresistance. *Nano Lett.* **2020**, *20*, 6815–6823. [[CrossRef](#)] [[PubMed](#)]
15. Wang, S.; Wang, W.; Zou, L.; Zhang, X.; Cai, J.; Sun, Z.; Shen, B.; Sun, J. Magnetic Tuning of the Photovoltaic Effect in Silicon-Based Schottky Junctions. *Adv. Mater.* **2014**, *26*, 8059–8064. [[CrossRef](#)]
16. Chen, P.; Jia, H.; Zhang, J.; Han, J.; Liu, X.; Qiu, J. Magnetic tuning of optical hysteresis behavior in lanthanide-doped nanoparticles. *J. Phys. Chem. C* **2015**, *119*, 5583–5588. [[CrossRef](#)]
17. Cai, K.; Yang, M.; Ju, H.; Wang, S.; Ji, Y.; Li, B.; Edmonds, K.W.; Sheng, Y.; Zhang, B.; Zhang, N.; et al. Electric field control of deterministic current-induced magnetization switching in a hybrid ferromagnetic/ferroelectric structure. *Nat. Mater.* **2017**, *16*, 712–716. [[CrossRef](#)]
18. Li, Y.; Edmonds, K.W.; Liu, X.; Zheng, H.; Wang, K. Manipulation of magnetization by spin-orbit torque. *Adv. Quantum Technol.* **2019**, *2*, 1800052. [[CrossRef](#)]
19. Snezhko, A.; Aranson, I.S. Magnetic manipulation of self-assembled colloidal asters. *Nat. Mater.* **2011**, *10*, 698–703. [[CrossRef](#)]
20. Cao, Y.; Sheng, Y.; Edmonds, K.W.; Ji, Y.; Zheng, H.; Wang, K. Deterministic magnetization switching using lateral spin-orbit torque. *Adv. Mater.* **2020**, *32*, 1907929. [[CrossRef](#)]
21. Sengupta, P.; Bellotti, E. Photo-modulation of the spin Hall conductivity of mono-layer transition metal dichalcogenides. *Appl. Phys. Lett.* **2016**, *108*, 211104. [[CrossRef](#)]
22. Ignatyeva, D.O.; Karki, D.; Voronov, A.A.; Kozhaev, M.A.; Krichevsky, D.M.; Chernov, A.I.; Levy, M.; Belotelov, V.I. All-dielectric magnetic metasurface for advanced light control in dual polarizations combined with high-Q resonances. *Nat. Commun.* **2020**, *11*, 5487. [[CrossRef](#)] [[PubMed](#)]
23. Aoshima, K.I.; Funabashi, N.; Machida, K.; Miyamoto, Y.; Kuga, K.; Ishibashi, T.; Shimidzu, N.; Sato, F. Submicron magneto-optical spatial light modulation device for holographic displays driven by spin-polarized electrons. *J. Disp. Technol.* **2010**, *6*, 374–380. [[CrossRef](#)]
24. Zhou, H.; Luo, X.; Yuan, C.; Hong, A.; He, J.; Lei, W. Modulation ferromagnetism in multiferroic  $\text{BiFeO}_3$  nanocrystals via bandgap engineering. *Appl. Phys. Lett.* **2019**, *114*, 253101. [[CrossRef](#)]
25. Zhou, H.; An, Z.; Yuan, C.; Luo, X. Light-modulated ferromagnetism of strained  $\text{NiFe}_2\text{O}_4$  nanocrystals. *Ceram. Int.* **2019**, *45*, 13319–13323. [[CrossRef](#)]
26. Xie, J.; Qin, H.; Hao, Y.; Cheng, B.; Liu, W.; Liu, L.; Ren, S.; Zhou, G.; Ji, Z.; Hu, J. Light control of ferromagnetism in ZnO films on Pt substrate at room temperature. *Sci. Rep.* **2017**, *7*, 45642. [[CrossRef](#)]
27. Fitzsimmons, M.R.; Silva, T.J.; Crawford, T.M. Surface oxidation of permalloy thin films. *Phys. Rev. B* **2006**, *73*, 014420. [[CrossRef](#)]
28. Liu, P.; Ren, Y.; Ma, W.; Ma, J.; Du, Y. Degradation of shale gas produced water by magnetic porous  $\text{MFe}_2\text{O}_4$  (M=Cu, Ni, Co and Zn) heterogeneous catalyzed ozone. *Chem. Eng. J.* **2018**, *345*, 98–106. [[CrossRef](#)]
29. Bhosale, S.V.; Ekambe, P.S.; Bhoraskar, S.V.; Mathe, V.L. Effect of surface properties of  $\text{NiFe}_2\text{O}_4$  nanoparticles synthesized by dc thermal plasma route on antimicrobial activity. *Appl. Surf. Sci.* **2018**, *441*, 724–733. [[CrossRef](#)]
30. Raimundo, R.A.; Silva, V.D.; Medeiros, E.S.; Macedo, D.A.; Simões, T.A.; Gomes, U.U.; Morales, M.A.; Gomes, R.M. Multifunctional solution blown spun NiFe– $\text{NiFe}_2\text{O}_4$  composite nanofibers: Structure, magnetic properties and OER activity. *J. Phys. Chem. Solids* **2020**, *139*, 109325. [[CrossRef](#)]
31. Hsieh, C.T.; Chuah, X.F.; Huang, C.L.; Lin, H.W.; Chen, Y.A.; Lu, S.Y. NiFe/(Ni, Fe) $_3\text{S}_2$  core/shell nanowire arrays as outstanding catalysts for electrolytic water splitting at high current densities. *Small Methods* **2019**, *3*, 1900234. [[CrossRef](#)]

32. Zong, W.; Rao, D.; Guo, H.; Ouyang, Y.; Miao, Y.E.; Wang, W.; Wang, J.; Lai, F.; Liu, T. Gradient phosphorus-doping engineering and superficial amorphous reconstruction in NiFe<sub>2</sub>O<sub>4</sub> nanoarrays to enhance the oxygen evolution electrocatalysis. *Nanoscale* **2020**, *12*, 10977–10986. [[CrossRef](#)] [[PubMed](#)]
33. Grosvenor, A.P.; Biesinger, M.C.; Smart, R.S.C.; McIntyre, N.S. New interpretations of XPS spectra of nickel metal and oxides. *Surf. Sci.* **2006**, *600*, 1771–1779. [[CrossRef](#)]
34. Biesinger, M.C.; Payne, B.P.; Grosvenor, A.P.; Lau, L.W.; Gerson, A.R.; Smart, R.S.C. Resolving surface chemical states in XPS analysis of first row transition metals, oxides and hydroxides: Cr, Mn, Fe, Co and Ni. *Appl. Surf. Sci.* **2011**, *257*, 2717–2730. [[CrossRef](#)]
35. Kresse, G.; Furthmüller, J. Efficient iterative schemes for ab initio total-energy calculations using a plane-wave basis set. *Phys. Rev. B Condens. Matter Mater. Phys.* **1996**, *54*, 11169–11186. [[CrossRef](#)]
36. Ernzerhof, M.; Scuseria, G.E. Assessment of the Perdew–Burke–Ernzerhof exchange–correlation functional. *J. Chem. Phys.* **1999**, *110*, 5029–5036. [[CrossRef](#)]
37. Hammer, B.; Hansen, L.B.; Norskov, J.K. Improved adsorption energetics within density-functional theory using revised Perdew–Burke–Ernzerhof functionals. *Phys. Rev. B Condens. Matter Mater. Phys.* **1999**, *59*, 7413–7421. [[CrossRef](#)]